Pergamon

Acta mater. 48 (2000) 4293–4306

Acta MATERIALIA

www.elsevier.com/locate/actamat

DETERMINATION OF PROPERTIES OF GRADED MATERIALS BY INVERSE ANALYSIS AND INSTRUMENTED INDENTATION

T. NAKAMURA[1]*, T. WANG[1] and S. SAMPATH[2]

[1]Department of Mechanical Engineering, State University of New York at Stony Brook, Stony Brook, NY 11794, USA and [2]Department of Materials Science and Engineering, State University of New York at Stony Brook, Stony Brook, NY 11794, USA

(Received 17 April 2000; received in revised form 6 July 2000; accepted 6 July 2000)

Abstract—In this paper, a new measurement procedure based on inverse analysis and instrumented micro-indentation is introduced. The inverse analysis is utilized to extract information from indented load–displacement data beyond usual parameters such as elastic modulus. For the initial implementation of this procedure, determination of non-linear functionally graded materials (FGMs) parameters is considered. In FGMs, the compositional profile and the effective mechanical property through the thickness are essential in verifying the fabrication process and estimating residual stresses and failure strengths. However, due to spatial variation of their properties, it is often difficult or costly to make direct measurements of these parameters. In order to alleviate the difficulties associated with testing of FGMs, we propose an effective but simple procedure based on the inverse analysis which relies solely on instrumented micro-indentation records. More specifically, the Kalman filter technique, which was originally introduced for signal/digital filter processing, is used to estimate FGM through-thickness compositional variation and a rule-of-mixtures parameter that defines effective properties of FGMs. Essentially, the inverse analysis processes the indented displacement record at several load magnitudes and attempts to make best estimates of the unknown parameters. Our feasibility study shows promising results when combined data from two differently sized indenters are employed. The procedure proposed is also applicable in estimating other physical and mechanical properties of any coating/layered materials.

Keywords: Functionally graded materials (FGM); Coating; Mechanical properties (plastic); Inverse analysis

1. INTRODUCTION

Functionally graded materials (FGMs) are spatial composites that display discrete or continuously varying compositions over a definable geometrical length. The gradients can be continuous on a microscopic level or layers comprised of metals, ceramics and polymers. In a typical FGM, the volume fractions of the constituents are varied gradually over a macroscale geometrical dimension such as coating thickness. Within an FGM, the different phases have different functions to suit the needs of the material. FGMs can be fabricated by several techniques including adhesive bonding, sintering, thermal spray and reactive infiltration [1, 2].

The material gradients induced by the spatial variations of the material properties make FGMs behave differently from common homogeneous materials and traditional composites. Because of this behavior, quantification of material parameters is more difficult. Recently, several methods have been introduced to characterize the properties of FGMs. Weissenbek *et al.* [3] applied a matrix-inclusion model based on the Mori–Tanaka method to define the rule of mixtures for a ceramic/metal system. Suresh *et al.* [4] and Giannakopoulos and Suresh [5, 6] have developed analytical and experimental tools to estimate the elastic properties of graded materials using instrumented micro-indentation. Other efforts on mechanical characterization of FGMs include the thermal residual stresses at the graded interface [7], the process-induced residual stresses [8], the Hertzian-crack suppression [9] and the crack-tip field in an elastic medium with varying Young's modulus [10]. Many other works are referenced in [2].

The measurement of *non-linear* or *elastic–plastic* FGMs is more complex due to additional material parameters. Unlike elastic FGMs, not only the elastic modulus but also the flow stress and the plastic strain-hardening modulus, which vary spatially, must be identified. In order to overcome the complexities

* To whom all correspondence should be addressed. Tel.: +1 (631) 632-8312; fax: +1 (631) 632-8544.

E-mail address: toshio.nakamura@sunysb.edu (T. Nakamura)

1359-6454/00/$20.00
PII: S1359-6454(00)00217-2

associated with the measurements of non-linear FGMs, we propose a new procedure that requires minimal effort in estimating the parameters. This procedure is based on the inverse analysis, which maximizes the extraction of information available in the micro-indentation data. Here, the Kalman filter theory is utilized to estimate the FGM's through-thickness compositional profile and the stress–strain transfer parameter that defines the effective properties of elastic–plastic FGMs. In order to implement the inverse analysis, the compositional profile is idealized to follow the power-law distribution and the effective property is defined by the rule of mixtures.

2. KALMAN FILTER

The Kalman filter was developed as an optimal, recursive, signal-processing algorithm [11]. Since then, due in large part to advances in digital computing, the Kalman filter has been the subject of extensive research and application. This inverse procedure has been applied in signal processing, inertial navigation, radar tracking, sensor calibration, manufacturing and other aspects [12]. It provides an efficient computational solution based on the least-squares theory. The method is effective in estimating unknown state variables using measurements that may contain substantial *error* or *noise*. Essentially, the algorithm updates the previous estimates through indirect measurements of the state variables and the covariance information of both the state and measurement variables.

The theory of the Kalman filter is based on the following update algorithm

$$\boldsymbol{x}_t = \boldsymbol{x}_{t-1} + \boldsymbol{K}_t[\boldsymbol{z}_t - \boldsymbol{H}_t(\boldsymbol{x}_{t-1})]. \tag{1}$$

Here, $\boldsymbol{x}_t$ is the state vector containing *unknown parameters*, z_t is the vector containing *experimentally measured variables* and $\boldsymbol{H}_t$ is the vector for the measurement variables shown as functions of state parameters. The subscript "*t*" denotes updating increment. It is assumed that $\boldsymbol{z}_t$ contains measurement error while the exact relation between the state parameters (e.g., material constants) and the measured variables (e.g., displacement record) is given in the function $\boldsymbol{H}_t$. The correction at each increment is made through the Kalman gain matrix $\boldsymbol{K}_t$ calculated as

$$\boldsymbol{K}_t = \boldsymbol{P}_t \boldsymbol{h}_t^{\mathrm{T}} \boldsymbol{R}_t^{-1}, \quad \text{where} \tag{2}$$
$$\boldsymbol{P}_t = \boldsymbol{P}_{t-1} - \boldsymbol{P}_{t-1}\boldsymbol{h}_t^{\mathrm{T}}(\boldsymbol{h}_t \boldsymbol{P}_{t-1}\boldsymbol{h}_t^{\mathrm{T}} + \boldsymbol{R}_t)^{-1}\boldsymbol{h}_t \boldsymbol{P}_{t-1}.$$

Here, $\boldsymbol{P}_t$ is the measurement covariance matrix related to the range of unknown state parameters at increment *t*. Also, $\boldsymbol{R}_t$ is the error covariance matrix which is related to the size of the measurement error. While the former matrix is updated every increment according to equation (2), the values of the latter matrix must be prescribed at each increment. The matrix $\boldsymbol{h}_t$ contains the gradients of $\boldsymbol{H}_t$ with respect to $\boldsymbol{x}_t$. Both $\boldsymbol{H}_t$ and $\boldsymbol{h}_t$ functions must be known *a priori*.

The Kalman filter has been used in seeking unknown parameters of homogeneous material models [13–15]. Essentially, this inverse analysis post-processes experimentally obtained data and attempts to best estimate unknown state variables or material constants. In our analysis, the Kalman filter technique is employed for the determination of elastic–plastic FGM parameters using instrumented indentation. The following information is required for the procedure: measured indented load–displacement records and displacement as a function of load for given material parameters. In the Kalman filter procedure, it is known that the convergence characteristics depend on several factors including shape of the test specimen, initial estimates of the unknown parameters and the measurement error, as well as the accuracy of $\boldsymbol{H}_t$ and $\boldsymbol{h}_t$ functions.

In order to establish an effective procedure based on the Kalman filter, the following tasks must be performed.

1. Representation of the unknown variables in suitable forms.
2. Selection of appropriate ranges/domain sizes for unknown variables.
3. Creation of reference data source/table for the measurement variables and their gradients.
4. Choice of total number of filtering increments and their magnitudes.
5. Determination of suitable values for the matrices of covariant $\boldsymbol{P}_t$ and $\boldsymbol{R}_t$.

The above tasks are carefully examined and discussed in the following sections. Many inverse problems are initially "ill-posed", which means that convergence to the correct solutions is difficult. Therefore, it is required to formulate "a priori information" and/or supply additional information/measurements to improve the estimates.

3. GEOMETRICAL AND MATERIAL MODELS

3.1. Micro-indentation test

In our effort to establish a useful but robust procedure to determine the properties of FGMs, a thin FGM model placed on top of a thick substrate as shown in Fig. 1 is considered. Although there are various methods to measure mechanical responses of FGMs, including optical techniques and strain gages, an instrumented micro-indentation, whose requirements for specimen preparation are minimal, is chosen. The instrumented indenter can be used to generate a continuous indented load–displacement record of any sufficiently flat specimen. In other experimental procedures, specimen preparation is

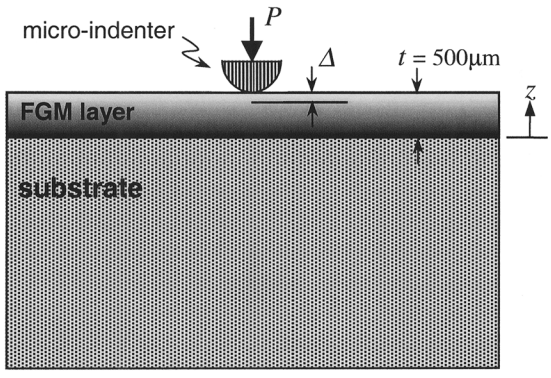

Fig. 1. Schematic illustration of spherical micro-indentation of an FGM layer on a thick substrate. The FGM thickness is 500 μm, the indenter force is P and the indented displacement is Δ.

more difficult and may also alter FGMs by releasing residual stresses and/or inducing micro-damages. Although the indentation method has been widely used to determine elastic modulus and hardness, it has been speculated that more useful information can be extracted from indented force–displacement data. Recently, using instrumented micro-indentation records, Suresh and Giannakopoulos [16, 17] introduced effective procedures to examine the residual stresses and the elastic–plastic properties of homogeneous materials. Others have also proposed indentation techniques to measure mechanical properties of various materials including plasma-sprayed coatings [4, 18–20]. Our proposed indentation procedure attempts to identify the complex elastic–plastic FGM properties through the use of the inverse analysis technique. This Kalman filter requires only indentation records although any additional measurements such as strains from gages would improve the accuracy. In general, any additional types of measurement enhance the convergence rate of unknown parameters. In our study, however, other measurement types are not considered since they would require extra experimental efforts. Our aim is to develop an effective procedure with a relatively simple experimental procedure.

The FGM layer considered here is made up of two phases: ceramic and metal. For the ceramic phase, we have assumed a model similar to that of yttria partially stabilized zirconia (PSZ) while the metal phase is assumed to be a bond metal (e.g., NiCrAlY). In our analysis the ceramic is assumed to be linear elastic with $E = 50$ GPa and $\nu = 0.25$, while the metal is modeled as a bi-linear elastic–plastic material with $E = 30$ GPa, $\nu = 0.25$, $\sigma_y = 50$ MPa and $H = 5$ GPa [21]. At any material location where two phases coexist, its behavior is elastic–plastic. Although these material constants correspond to thermally sprayed coatings, any other values are applicable. These are simply model parameters. No anisotropic effect is included in the present study. The steel substrate is assumed to be elastic since it is never subjected to large stresses during the indentation of interest. The spherical indenter is assumed to be made of a hard material (e.g., tungsten carbide with $E = 614$ GPa and $\nu = 0.22$). Initially, its radius is set at $r = 100$ μm. Unknown FGM parameters to be sought in the inverse analysis are described in the following sections.

3.2. Through-thickness compositional variation

One of the key parameters needed to be determined after fabrication of FGMs is the composition of multiple phases through the thickness. In the case of thermal barrier coatings, it is desirable to maximize the ceramic content to enhance the thermal insulation without sacrificing the beneficial mechanical aspects of the graded regions. In such a case, a parabolic profile would be suitable. In other applications, a linear profile may be optimal. Synthesis of a desired grading profile depends on the deposition efficiency and requires integration of processing hardware, material behavior and micro characteristics. In general, it is difficult to precisely deposit different phases to form an FGM with desired compositional profile. Figure 2 shows FGMs consisting of PSZ and NiCrAlY [22]. In the thermal spray process, a discrepancy in the deposit efficiencies of the two components causes a difference in target and measured mixture ratios. In order to measure the composition of phases at a given location or through the thickness, an FGM specimen must be carefully inspected. Usually an image analysis and/or X-ray diffraction is needed to measure the compositional variation. The proposed inverse analysis may simplify this process.

In our analysis, it is assumed that the compositional variation of ceramic and metal phases can be approximated by an idealized power-law equation as

$$V_c = (z/t)^n. \tag{3}$$

Here, V_c is the volume fraction of the ceramic phase, z is the location measured from the interface with the substrate, t is the total thickness of the FGM layer, and n is the power exponent. Note that, at any location, $V_c + V_m = 1$, where V_m is the volume fraction of the metal phase. In our model, the composition is pure ceramic at the top ($z = t$) while it is pure metal at the interface ($z = 0$). The unknown state variable to be sought in the inverse analysis is the power exponent n, which directly controls the through-thickness variation of volume fraction. When $n = 1$, the composition changes linearly through the thickness while $n = 1/2$ or 2 corresponds to the quadratic or parabolic distribution. Since we need to specify a likely range of the unknown variable in the inverse analysis, it is assumed that n ranges from 1/3 to 3. Any value outside this range is not usually desired since such an FGM would contain too much of one phase. (When $n = 1/3$ or 3, one phase has 75% of the total volume.) The profiles of the through-thickness compositional variation for different n are shown in Fig. 3.

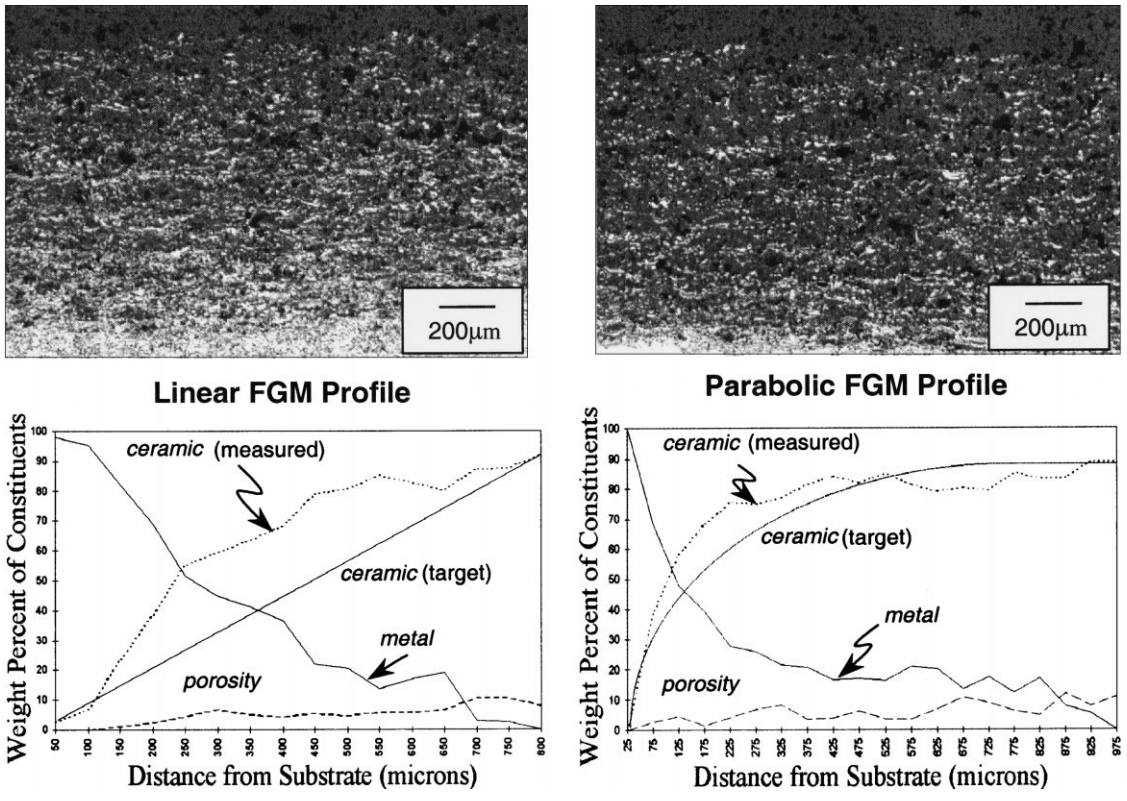

Fig. 2. Cross-sectional micrographs and corresponding composition profiles of FGMs containing ceramic (PSZ) and metal (NiCrAlY) phases [22].

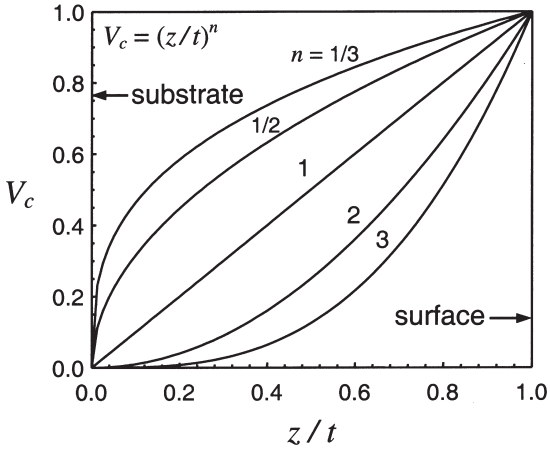

Fig. 3. Variations of ceramic volume fraction through-thickness for various power-law exponents, ranging from 1/3 to 3. The surface of the FGM is at $z = t$ while the interface with the substrate is at $z = 0$.

3.3. Effective mechanical properties of FGM

Another important variable in FGMs is a parameter that defines the effective mechanical property of the two-phase composite. With a certain mixture of ceramic and metal phases, the response of the composite is dependent upon factors such as the concentration, shape and contiguity, and spatial distribution of each phase. There are two extreme rule-of-mixtures models to describe the effective mechanical properties of a composite comprising two elastically isotropic constituent phases: the Voigt and Reuss models. The Voigt model corresponds to the case when the applied load causes equal strains in the two phases. The overall composite stress is the sum of stresses carried by each phase. Therefore, the overall Young's modulus is the average of the constituents' moduli weighted by the volume fraction of each phase as

$$E_f = E_c V_c + E_m V_m, \tag{4}$$

where E is the Young's modulus. The subscripts f, c and m denote FGM composite, ceramic and metal, respectively. The Reuss model corresponds to the case when each phase of the composite carries an equal stress. The overall strain in the composite is the sum of the net strain carried by each phase, and the effective Young's modulus is given by

$$E_f = \left(\frac{V_c}{E_c} + \frac{V_m}{E_m} \right)^{-1}. \tag{5}$$

In many composites, the actual effective modulus falls between the two extreme models shown in equations (4) and (5).

In the current analysis, the so-called "modified rule

of mixtures" described in [2, 7, 23, 24] is adopted. If the composite is treated as isotropic, its uniaxial stress and strain can be decomposed into

$$\sigma_f = V_c\sigma_c + V_m\sigma_m \quad \text{and} \quad \varepsilon_f = V_c\varepsilon_c + V_m\varepsilon_m, \quad (6)$$

where σ_c, σ_m and ε_c, ε_m are the stresses and strains of the ceramic and metal under uniaxial stress and strain conditions. The normalized ratio of the stress to strain transfer is then defined by a dimensionless parameter

$$q = \frac{1}{E_c}\frac{\sigma_c - \sigma_m}{\varepsilon_c - \varepsilon_m}, \quad (7)$$

where $0 \le q \le \infty$. Combining equations (6) and (7) and setting $E_f = \sigma_f/\varepsilon_f$, one may obtain the following expression for the effective modulus

$$E_f = \frac{V_cE_c + V_mE_mR}{V_c + V_mR}, \quad \text{where } R = \frac{q+1}{q + E_m/E_c}. \quad (8)$$

Here, choosing the stress–strain transfer parameter $q \to 0$ recovers the Reuss model and $q \to \infty$ refers to the Voigt model. The above expressions suggest that the single parameter q plays a key role in defining the effective mechanical properties of the composite. In general, q is an empirical parameter that depends on many factors including composition, microstructural arrangement, internal constraints, and others. The exact nature of this dependence, however, is not yet well known. A similar rule can be established for the effective Poisson's ratio. However, in our analysis, the Poisson's ratios are assumed to be constant in both phases and not vary throughout the FGM. The modified rule of mixtures can be extended to elastic–plastic composites [2]. If we consider an elastic ceramic phase and an elastic–plastic metal phase, the effective or overall yield stress σ_{yf} of the composite may be expressed as

$$\sigma_{yf} = \sigma_{ym}\left(V_m + \frac{E_cV_c}{E_mR}\right), \quad (9)$$

where σ_{ym} is the yield stress of the pure metal phase. The effective strain-hardening coefficient of the composite can be also expressed with q as

$$H_f = \frac{V_cE_c + V_mH_mR'}{V_c + V_mR'}, \quad \text{where } R' = \frac{q+1}{q + H_m/E_c}, \quad (10)$$

where H_m is the plastic tangent modulus of the metal phase. If the stress–strain transfer variable q and the volume fractions are known, the above formulations can be used to describe the complete effective mechanical properties of the composite. Although there are other formulations that are more complex, this approach requires only the single parameter to be determined. The stress–strain relations of the composite with equal mixture (i.e., $V_c = 0.5$, $V_m = 0.5$) for various q are shown in Fig. 4. The large span of stress–strain curves indicates the flexibility of this modified rule of mixtures. Stress–strain relations of many composites should fall within this range. In reality, it is possible that the variable q may be a function of volume fraction [i.e., $q(V_c)$]. This means as the volume fractions of constituents vary within FGMs, its value may also change. However, such a dependence is not considered, and q is assumed to be constant through the thickness and independent of the compositional ratio in the present analysis.

3.4. Suitable representations of FGM parameters

In the previous two sections, we described two key parameters that characterize the properties of the FGM layer. These parameters will be treated as the unknown state parameters in the Kalman filter. However, direct implementations of these parameters are not suitable in the Kalman filter due to different ranges of n and q to explore ($1/3 \le n \le 3$, $0 \le q \le \infty$). In order to perform the procedure in a more consistent way, these parameters are re-formulated as

$$N = \frac{\log n}{2 \log 3} \quad \text{and} \quad Q = \sqrt{1 - e^{-q}}. \quad (11)$$

The above representations make the ranges of unknown parameters to be $-0.5 \le N \le 0.5$ and $0 \le Q \le 1.0$, respectively (i.e., 1×1 domain). In choosing these expressions, the records of load–displacement

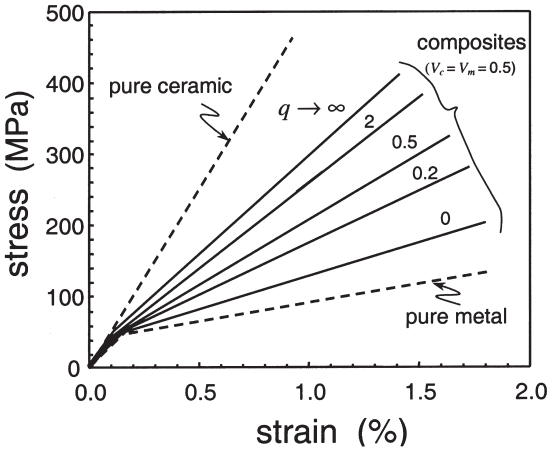

Fig. 4. Uniaxial stress–strain relations of an equal-mixture composite ($V_c = V_m = 0.5$) for various values of the stress–strain transfer parameter q. Note the large flexibility in the effective property. The dashed lines correspond to pure ceramic and metal, respectively.

for different n and q are closely monitored so that their variations are smoother over the domain of N and Q.

4. INVERSE ANALYSIS PROCEDURE

4.1. Application of Kalman filter in FGM model

Based on the previous sections, the components of the state vector or the unknown FGM parameters are defined as $\boldsymbol{x}_t = (Q_t, N_t)^{\mathrm{T}}$, where Q_t and N_t represent the estimates at time t. In our analysis, we assume the indenter load to be specified at a time increment (i.e., $P = P_1, P_2, P_3, \ldots$ at $t = 1, 2, 3, \ldots$) while the indented displacement Δ is the measured parameter. Alternatively, one may choose P to be the measured parameter instead of Δ. According to this arrangement, the vector containing measured variables in equation (1) can be set as $\boldsymbol{z}_t = \boldsymbol{\Delta}_t^{\mathrm{meas}}$, where the measured displacement may contain error/noise as $\boldsymbol{\Delta}_t^{\mathrm{meas}} = \boldsymbol{\Delta}_t + \boldsymbol{\Delta}_t^{\mathrm{err}}$. Here, $\boldsymbol{\Delta}_t$ is the exact or known displacement vector at load P_t, and the vector $\boldsymbol{\Delta}_t^{\mathrm{err}}$ contains measurement noise (within an error bound). Furthermore, the vector $\boldsymbol{H}_t$ in equation (1) can be shown as $\boldsymbol{H}_t = \boldsymbol{\Delta}_t(Q_{t-1}, N_{t-1})$, where Q_{t-1} and N_{t-1} correspond to most recent estimates of the state parameters. In equation (2), $\boldsymbol{h}_t$ is the displacement gradient with respect to Q and N.

The dimensions of vectors and matrices depend on the total number of P–Δ curves used in the Kalman filter. Initially a record from a single indenter is considered. In this case, $\boldsymbol{\Delta}_t = (\Delta_t)$. In a separate analysis when we consider two separate P–Δ records from two indenters (described in Section 5.2), $\boldsymbol{\Delta}_t = (\Delta_t^{\mathrm{A}}, \Delta_t^{\mathrm{B}})^{\mathrm{T}}$. Here the two indenters are denoted as A and B, respectively. The subscript t indicates the load increment/magnitude. Using these relations, equation (1) can be customized for the present procedure as

$$\boldsymbol{x}_t = \boldsymbol{x}_{t-1} + \boldsymbol{K}_t[\boldsymbol{\Delta}_t^{\mathrm{meas}} - \boldsymbol{\Delta}_t(\boldsymbol{x}_{t-1})], \tag{12}$$

where the Kalman gain matrix $\boldsymbol{K}_t$ is computed as

$$\boldsymbol{K}_t = \boldsymbol{P}_t\boldsymbol{\delta}_t^{\mathrm{T}}\boldsymbol{R}_t^{-1}, \quad \text{where} \qquad \boldsymbol{P}_t = \boldsymbol{P}_{t-1} - \boldsymbol{P}_{t-1}\boldsymbol{\delta}_t^{\mathrm{T}}(\boldsymbol{\delta}_t\boldsymbol{P}_{t-1}\boldsymbol{\delta}_t^{\mathrm{T}} + \boldsymbol{R}_t)^{-1}\boldsymbol{\delta}_t\boldsymbol{P}_{t-1}. \tag{13}$$

Also, the displacement gradient matrix $\boldsymbol{\delta}_t$ can be shown as

$$\boldsymbol{\delta}_t = \frac{\partial \boldsymbol{\Delta}_t}{\partial \boldsymbol{x}_t} = \begin{cases} \left(\dfrac{\partial \Delta_t}{\partial Q} \quad \dfrac{\partial \Delta_t}{\partial N}\right) & \text{for one indenter} \\ \begin{pmatrix} \dfrac{\partial \Delta_t^{\mathrm{A}}}{\partial Q} & \dfrac{\partial \Delta_t^{\mathrm{A}}}{\partial N} \\ \dfrac{\partial \Delta_t^{\mathrm{B}}}{\partial Q} & \dfrac{\partial \Delta_t^{\mathrm{B}}}{\partial N} \end{pmatrix} & \text{for two indenters} \end{cases} \tag{14}$$

In the above equation, the matrix $\boldsymbol{\delta}_t$ is shown for both one indenter and two indenter cases. Also in equation (13), the two matrices of covariance are chosen as

$$\boldsymbol{P}_0 = \begin{pmatrix} (\Delta Q)^2 & 0 \\ 0 & (\Delta N)^2 \end{pmatrix} \quad \text{and} \quad \boldsymbol{R}_t = \begin{cases} R^2 & \text{for one indenter} \\ \begin{pmatrix} R^2 & 0 \\ 0 & R^2 \end{pmatrix} & \text{for two indenters} \end{cases} \tag{15}$$

In the initial matrix of measurement covariance $\boldsymbol{P}_0$, $\Delta Q = Q_{\max} - Q_{\min}$ and $\Delta N = N_{\max} - N_{\min}$ (i.e., $\Delta Q = \Delta N = 1$ in the present case). While $\boldsymbol{P}_0$ is diagonal, the procedure fills $\boldsymbol{P}_t$ to a matrix during subsequent increments. In the error covariance matrix $\boldsymbol{R}_t$, R is generally set close to the estimated maximum measurement error as $R = |\Delta_t^{\mathrm{err}}|_{\max}$. The suitability of this value is examined and discussed in Section 5.3. When the error bound or measurement tolerance (white noise) is assumed to be constant throughout the loading, R can be set constant and independent of t as in the present analysis. In many inverse problems, the errors from multiple measurements can be interdependent and $\boldsymbol{R}_t$ can be a full matrix. The increments are carried out for $t = 1, 2, \ldots, t_{\max}$. The state vector $\boldsymbol{x}_t$ at $t_{\max}$ contains the final estimates of Q and N from the Kalman filter. The above procedure is illustrated by the flow chart shown in Fig. 5. This Kalman filter procedure is implemented in a computational code.

4.2. Computational model

A detailed finite element analysis is carried out to verify the proposed procedure. The micro-indentation on the FGM layer on a thick steel substrate is modeled using axisymmetric elements. The mesh shown in Fig. 6 is carefully constructed after several trial calculations. In order to obtain smooth P–Δ responses, it is essential to have small elements at the contact area. These elements are needed to accurately resolve high stresses and the evolving contact condition. Larger elements are used away from the contact although the maximum through-thickness length of elements within the FGM layer is kept at 10 μm. There are 64 element layers through the thickness of the FGM. Within each layer, the material properties are prescribed according to equations (3) and (8)–(10) for given n and q, respectively. Although the through-thickness property variation is element by element, the large number of layers should produce a sufficiently continuous variation. The element sizes of the spherical indenter are also kept small along the contact surface as shown. In the figure, the radius of the indenter is $r = 100$ μm. There is total of about 6600 four-noded isoparametric elements in the model.

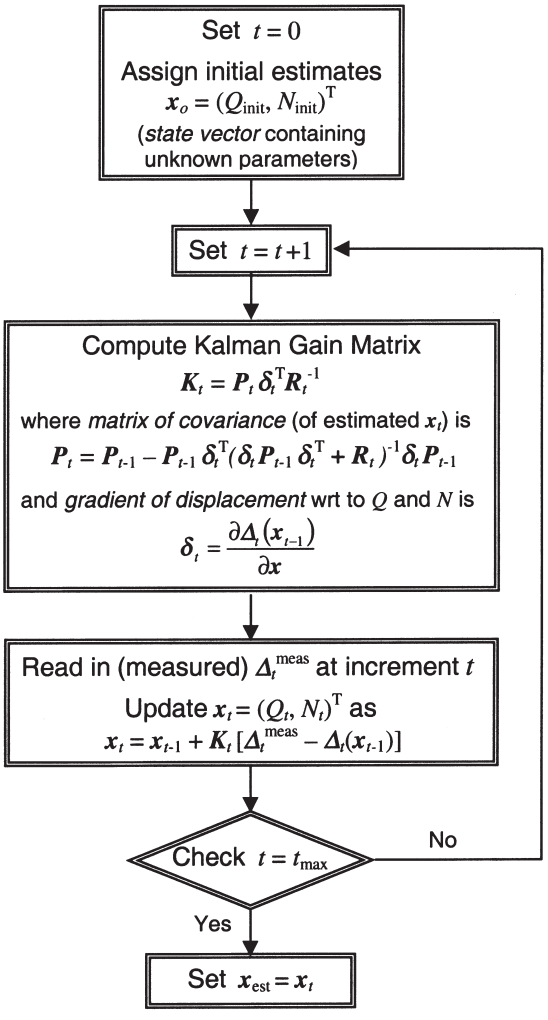

Fig. 5. Flow chart for the Kalman filter procedure to determine unknown parameters using the indented displacements at several load increments.

For the boundary condition, the radial displacement along the symmetry axis and the vertical displacement along the bottom of the substrate are constrained.

The loading to the FGM is simulated by gradually increasing the vertical displacement of nodes on the top surface of the semi-spherical indenter. Displacement-controlled loading is chosen because of its stable numerical convergence in contact simulations. The equivalent reaction force is reported as the load P. The indented displacement Δ is obtained from the vertical displacement of the contact node at the center. The difference between Δ and the prescribed displacement at the top of the indenter is very small since the indenter is much stiffer than the FGM layer. In addition, one may calibrate the displacement to account for the compliance of the steel substrate. However, such calibrated Δ is not used here since it would not influence the accuracy of the inverse analysis. The Kalman filter monitors the *change* of P–Δ curves and not the magnitude of Δ. In fact, displacement with the machine compliance can be also used as long as its contribution is included in the model. Since the indenter is much stiffer than the FGM layer, the contact radius ρ can be approximated as $\rho = \sqrt{2r\Delta}$, where r is the radius of indenter. At the minimum load of the Kalman filter used in the analysis, the contact area covers 12–17 elements since the smallest element size is 1.25 μm.

4.3. Creation of reference data source

Since the Kalman filter compares the measured data with known solutions, the P–Δ relation for given q and n, or Q and N, must be available. This relation can be obtained either analytically or numerically. In our proposed procedure, this information or the reference data source is generated by finite element calculations since no closed-form solution exists for elastic–plastic FGMs. By varying the values of Q and N, stiff to compliant responses can be obtained. Figure 7 shows P–Δ relations of FGMs with four different sets of Q and N. In each calculation, the prescribed displacement is increased by increments of 0.1 μm. Various responses of the FGMs are also illustrated by the shades of equivalent plastic strain in Fig. 8. Here, shaded areas represent plastic zones and larger plastic strains are shown by darker shades. All of the models are under the same indented load at $P = 2$ N. Note the significant differences in the plastic zone sizes under the same load. The plastic zone of the compliant model ($Q = 0$, $N = -0.5$) is more than twice as large as that of the stiff model ($Q = 1$, $N = 0.5$). Regardless of the model, the plastic zone is confined to a region immediately underneath the indenter. Since the FGM thickness is 500 μm, the plastic zones occupy small fractions of the thickness.

As shown in equations (12) and (13), the Kalman filter requires Δ and its derivatives with respect to Q and N at load P. These values can be determined by carrying out many finite element calculations for various sets of Q and N. In order to minimize such computational effort, we adopt cubic Lagrangian interpolation functions to calculate the displacement and its gradients. Sixteen points in the Q–N domain are chosen as the base points whose values are used in the calculations. These points are uniformly distributed in the Q–N domain as shown in Fig. 9. After 16 separate finite element calculations are carried out, the displacements and their gradients for any Q and N can be obtained through the cubic Lagrangian interpolation functions. Initially bi-quadratic functions at 3×3 points were employed. However, the accuracy was not sufficient and we tried bi-cubic functions at 4×4 points. These higher-order functions enabled interpolated Δ to achieve 0.2% accuracy for any combination of Q and N. The interpolated Δ for various Q and N at the load level of $P = 0.6$ N is shown in Fig. 10.

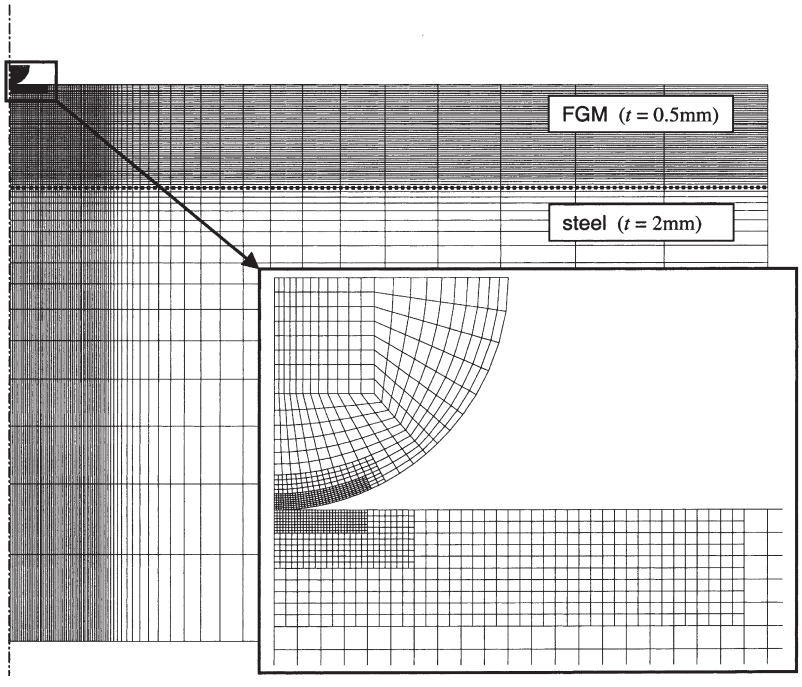

Fig. 6. The axisymmetrical finite element mesh for an indented FGM on a substrate. The near-contact region with smaller elements is enlarged for clarity.

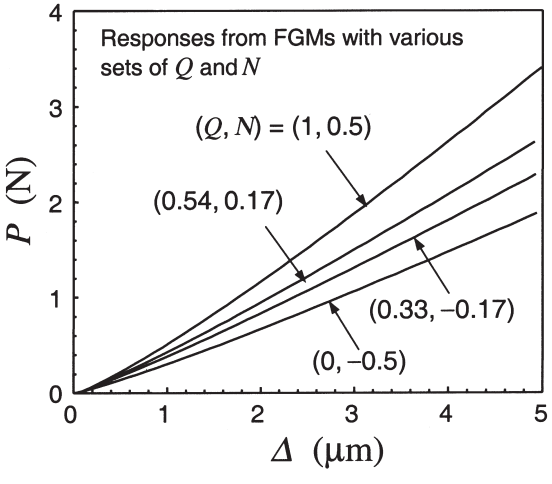

Fig. 7. Indented load–displacement curves of FGMs with various Q and N. Stiff to compliant responses can be observed with different parameters.

5. IDENTIFICATION OF FGM PARAMETERS

5.1. Single indenter procedure

The inverse method uses the experimentally measured displacement at several load increments to seek for the unknown parameters. Before applying this method in a real experiment, it is necessary to verify and quantify the accuracy of this procedure. This task is carried out with simulated experimental data generated from the finite element solutions. The simulation study allows us to make direct evaluations of estimated solutions with respect to actual solutions. At first, an arbitrary set of Q and N is chosen for the FGM model and the indentation process is simulated. Then suitable load increments for the displacement measurements are selected. After several trials, 15 load increments ranging from $P = 0.6$ N to 2.0 N with interval of 0.1 N are chosen. In order to replicate experimental white noise, *random* errors within a bound are added to these 15 displacement records. The error bound or tolerance of measurement is assumed to be $|\Delta_t^{\text{err}}|_{\max} = 0.05$ μm, which is about 1–4% of the indented displacements. Figure 11 shows the 15 simulated displacement records for the FGM with the properties $Q = 0.43$ and $N = 0$.

Using these data as input, the Kalman filter process outlined in Fig. 5 is carried out. The component of the error covariance matrix $\boldsymbol{R}_t$ is set to be $R^2 = (0.05\ \mu\text{m})^2$, which equals the square of measurement tolerance. The Kalman filter also requires initial estimates to be assigned to the unknown parameters. Figure 12(a) shows the converging trends of two sets of arbitrarily chosen initial values, denoted as A with $Q_{\text{init}} = 0.25$, $N_{\text{init}} = -0.15$ and B with $Q_{\text{init}} = 0.25$, $N_{\text{init}} = 0.25$, respectively. The actual values of the FGM parameters are $Q_{\text{act}} = 0.43$, $N_{\text{act}} = 0$. The deviations between the estimated values and the actual values during the 15 increments are indicated in the figure. The results show that the set A never approaches the actual values while the other set, B, converges to the actual values within a few load increments. In Fig. 12(b), the convergence behavior is shown on the Q–N domain. Here two additional sets of initial estimates, C and D, are assigned in the inverse analysis. Each symbol indicates estimated

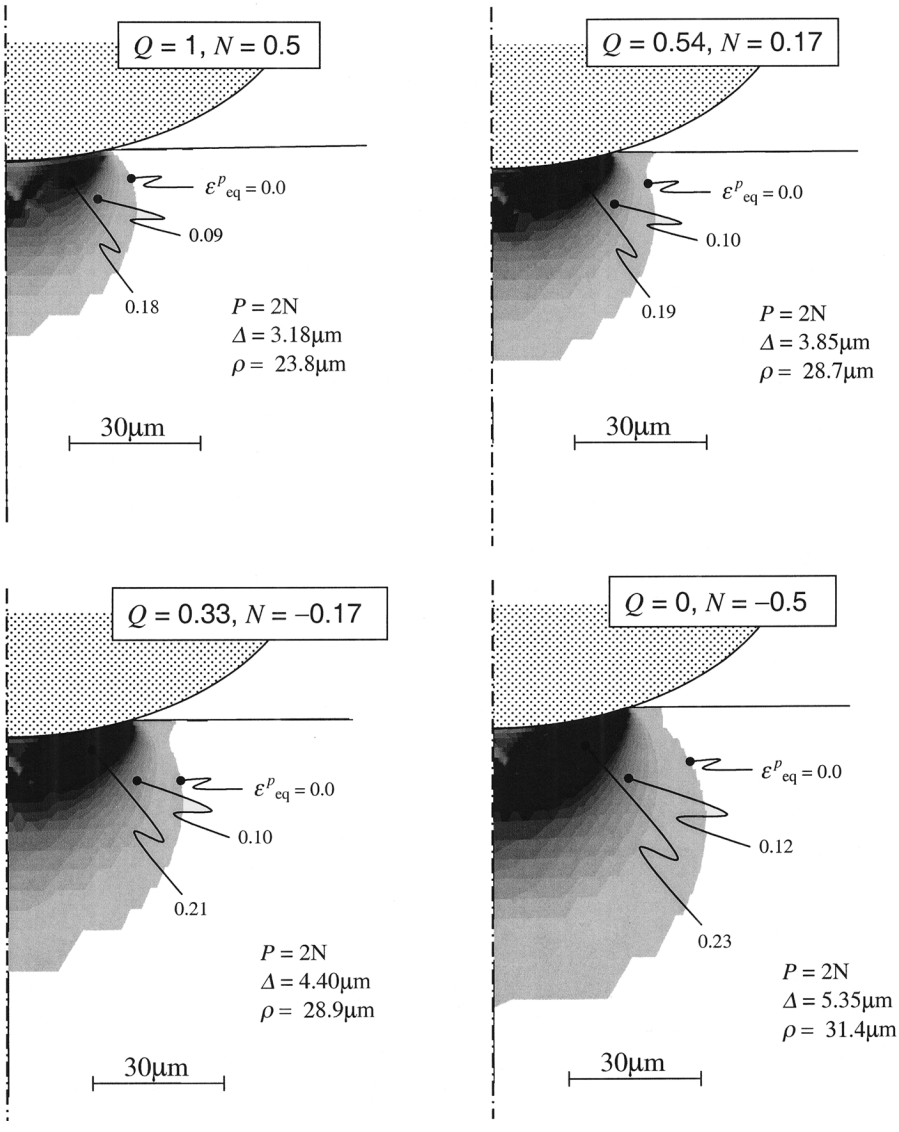

Fig. 8. Shades of equivalent plastic strain for FGMs with various sets of Q and N. Darker regions correspond to higher plastic strain. All models are under the same load, $P = 2$ N. Corresponding indented displacement (Δ) and radius of contact (ρ) are noted.

values of Q and N at an increment. This figure clearly shows the "approaching" trend of each estimate. The two initial estimates, B and D, continuously move towards the actual values while the others, A and C, never approach the actual solutions.

These results confirm that initial estimates play an important role in the convergence condition. However, in real tests, it would be impossible to determine whether the final estimates of Q and N are close to those of the actual FGM or not. Unlike the finite element simulation, the actual solutions are not known *a priori* in real FGMs. This means, in order for the inverse procedure to be useful, many initial estimates should lead to the exact solutions. We investigate this aspect by assigning many different initial estimates through the Kalman filter. The initial values of Q and N are varied every 0.025 within the Q–N domain (i.e., $41\times41 = 1681$ times in $0\leq Q\leq 1.0$, $-0.5\leq N\leq 0.5$). With every set of initial estimates, the deviation or error of its final estimates Q_{est} and N_{est} are computed as

$$\text{error} = \sqrt{\left(\frac{Q_{\text{est}}-Q_{\text{act}}}{\Delta Q}\right)^2 + \left(\frac{N_{\text{est}}-N_{\text{act}}}{\Delta N}\right)^2}. \quad (16)$$

The results are shown as circles in Fig. 13. Here the shaded circles represent initial estimates whose final values came within 10% of the actual values, while the open circles are those that came within 15%. These circles essentially make up a "domain of convergence" for the Kalman filter. It can be observed that these circles form a strip along a diagonal direction. Such a phenomenon can be explained by the dis-

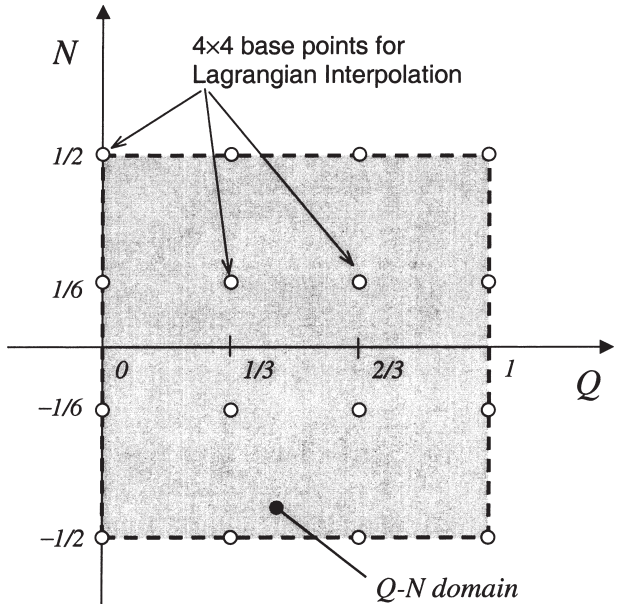

Fig. 9. Domain of unknown state variables ($0 \le Q \le 1.0$, $-0.5 \le N \le 0.5$). Cubic Lagrangian interpolation functions are used with the values at 4×4 base points.

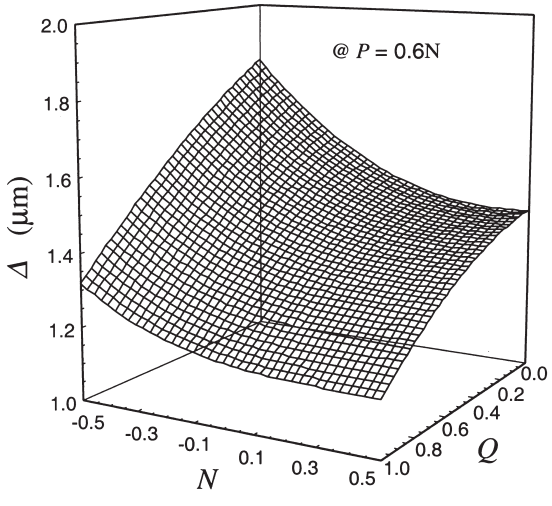

Fig. 10. Indented displacement at $P = 0.6$ N is shown as a function of Q and N. The displacement surface is constructed with interpolation functions.

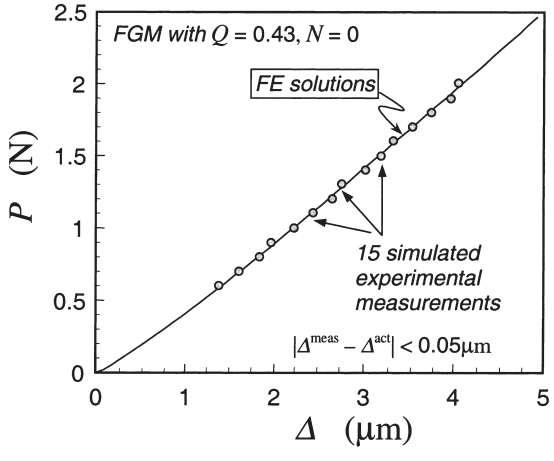

Fig. 11. Simulated displacement measurements are created by adding random errors to the finite element solutions. The maximum error/noise is set at 0.05 μm.

placement behavior shown in Fig. 10. In this figure, the displacement variation is much greater along the same diagonal direction as the domain of convergence shown in Fig. 13. In general, the Kalman filter is more sensitive when large changes occur in the measured variable. Regardless of the shape, the converged domain occupies less than 1/3 of the total Q–N area. This means that the majority of initial estimates never yield solutions close to the actual values. Such a procedure is not effective, and an improvement is necessary. One way to enhance the accuracy is to supply more measurement information to the Kalman filter as discussed next.

5.2. Double indenter procedure

As described earlier, our aim is to establish a method that requires minimal experimental effort. Although additional measurements from strain gages and optical methods should certainly improve the Kalman filter, they are not considered. Instead, other measurements from another indenter with a different radius are considered. It is assumed that different P–Δ characteristics can be obtained from such an indenter, and they are sufficient to improve the accuracy. The choice of new indenter radius is made carefully. Its size must be substantially different from the first one ($r = 100$ μm) while it cannot be too large compared with the layer thickness ($t = 500$ μm).

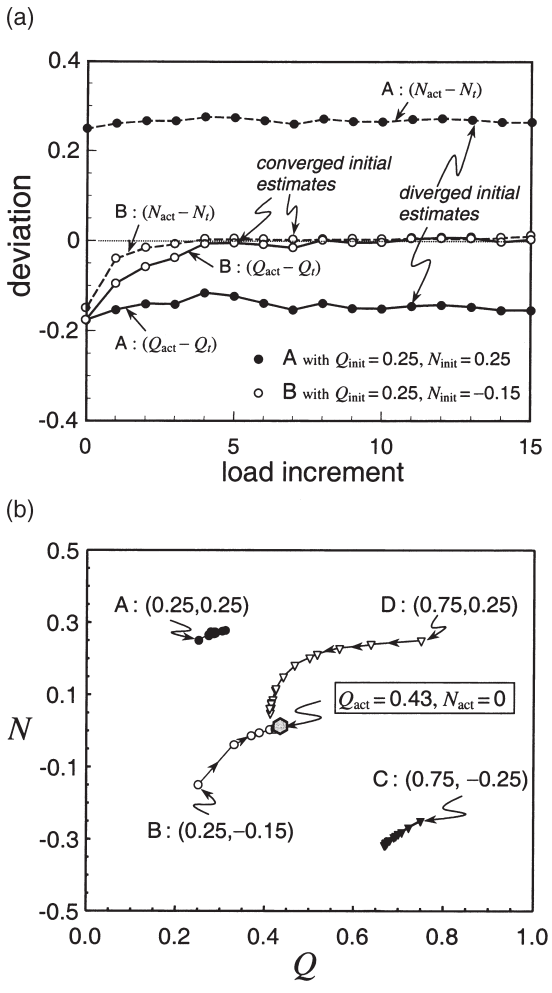

Fig. 12. Converging trends of different initial estimates. (a) Two cases shown as a function of load increments. (b) Four cases shown on the *Q*–*N* domain. The diverged cases (*A* and *C*) stay away from the actual values ($Q = 0.43$ and $N = 0$).

After several trials, the new radius is chosen to be $r = 500$ μm. The load increments for this large indenter are set between 5 and 12 N with 0.5 N intervals. At first, as in the smaller indenter, the reference data are created by carrying out separate finite element calculations with 16 sets of different *Q* and *N*. Again the loading to the FGM layer is applied through increasing the displacement of nodes on the top of the larger indenter. In the next step, actual measurements are simulated by adding random errors to the finite element solutions as shown in Fig. 14. The same measurement tolerance is used. Prior to running the Kalman filter using both small and large indenter data, the convergence behavior of the large indenter alone was inspected. The resulting domain of convergence was very similar to that of the small indenter shown in Fig. 13. It further confirms that single indenter results are not sufficient to obtain good convergence behavior.

The combined indenter procedure is carried out with the Kalman filter equations (12)–(15) for the two indenter case. With the additional measurement data, the dimensions of vectors and matrices increase. In the Kalman filter program, the reference *P*–*Δ* data for both small and large indenters are supplied initially. After initial estimates of *Q* and *N* are input, the program processes the two displacements of the first increment from the small and large indenters simultaneously (i.e., Δ^{meas} at 0.6 N for the small indenter and Δ^{meas} at 5 N for the large indenter). These values are used to update the estimates of *Q* and *N*. This process is repeated for 15 increments to obtain the best estimates in the current procedure. Note that the total numbers of load increments for the two indenters must be identical although the load magnitudes can be different. The major difference between the single and double indenter cases is that the Kalman filter uses larger rank tensors to process. This generally leads to better convergence characteristics.

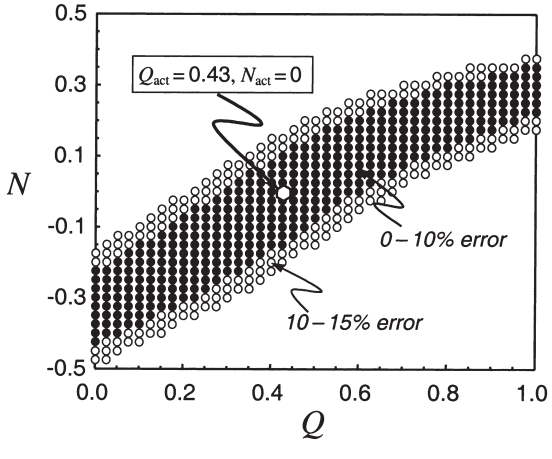

Fig. 13. Shaded circles correspond to initial estimates that achieved convergence within 10% of the actual values while open circles came within 15%. These circles make up the domain of convergence for the Kalman filter.

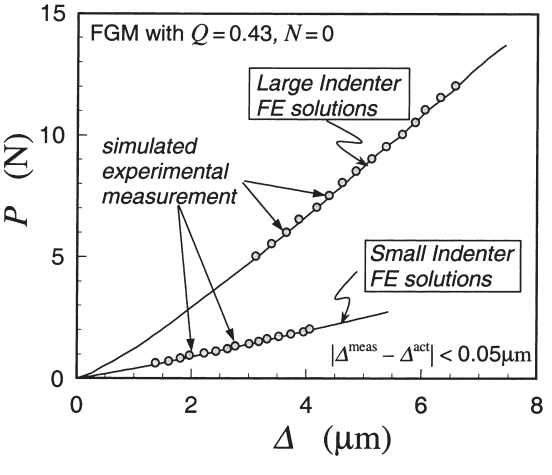

Fig. 14. Simulated displacement measurements from two indenters with different radii. The smaller one has $r = 100$ μm and the larger one has $r = 500$ μm. Random errors of up to 0.05 μm are added to the finite element solutions.

As in the single indenter case, its accuracy is evaluated by generating a domain of convergence. The results are shown in Fig. 15, where a dramatic improvement can be observed. Almost all of the initial estimates lead to actual solutions during the Kalman filter procedure. Alternatively, one can assign any initial values for Q and N in the Kalman filter to obtain very accurate estimates of Q and N. This result supports the usefulness of the proposed method. The feasibility of this method is also examined by choosing different Q_{act} and N_{act}. Their convergence behaviors are similar to the one in Fig. 15. When combined P–Δ data from the small and large indenters are used, more than 80% of initial estimates have achieved convergence to within 10% error of the actual solutions.

One of the major strengths of the Kalman filter is its ability to process data containing substantial measurement noises or errors. We examined this feature by re-creating simulated measurements with much greater random errors as shown in Fig. 16(a). Here, the measurement tolerance or the error bound is set at $|\Delta_t^{\text{err}}|_{\max} = 0.2$ μm in both small and larger indenter results. This magnitude is four times larger than in the previous cases and the error can be 3–15% of the displacements shown in Fig. 16(a). Using these data, the Kalman filter is carried out and the resulting domain of convergence is shown in Fig. 16(b). Obviously the accuracy is reduced due to the worsened data quality. However, the domain including the open circles has nearly maintained its size. More than 80% of the total Q and N domain is still covered by the filled or open circles. These results prove the strength of this method even when relatively large error/noise is present in the measurements.

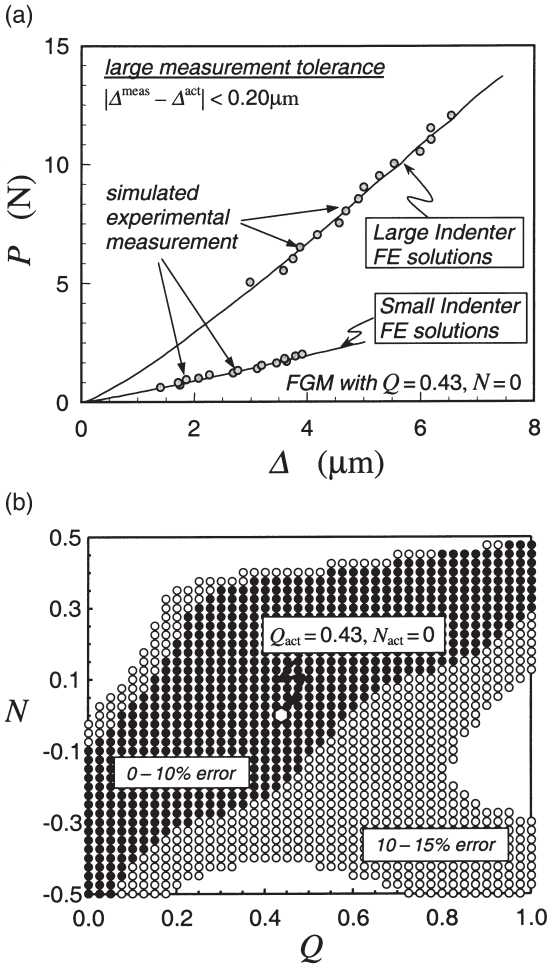

Fig. 16. (a) Simulated displacement measurements from two indenters with large random errors (tolerance) of up to 0.20 μm. (b) Domain of convergence obtained from the combined indenter case with large errors. Although the accuracy declines, the size is still large.

5.3. *Influence of covariant matrices*

During the study of this procedure, we have found that the values assigned to the error covariant matrix $\boldsymbol{R}_t$ influence the accuracy while initial values assigned to the measurement covariant matrix $\boldsymbol{P}_0$ have a very small effect. In all of the results shown previously, the components of $\boldsymbol{R}_t$ in equation (15) have been assigned as $R^2 = |\Delta_t^{\text{err}}|^2_{\max}$. However, it appears that other values may improve the convergence behavior of the Kalman filter. In order to optimize the Kalman filter procedure, different values are assigned to quantify the influences of $\boldsymbol{R}_t$. First, we carried out the procedure with the measurement data shown in Fig. 14. Here the measurement error bound or tolerance is set as $|\Delta_t^{\text{err}}|_{\max} = 0.05$ μm. Four separate cases with different R in $\boldsymbol{R}_t$ are carried out in the double indenter analysis. They are $R = 0.05$, 0.2, 0.5 and 2.0 μm, and identical initial estimates and actual solutions are assigned in all cases. The converging trends of these cases at each load increment are shown in Fig. 17(a). The normalized error is calculated by equation (14). In general, when large R is assigned, the convergence is steady but slow. On the other hand, if small R is

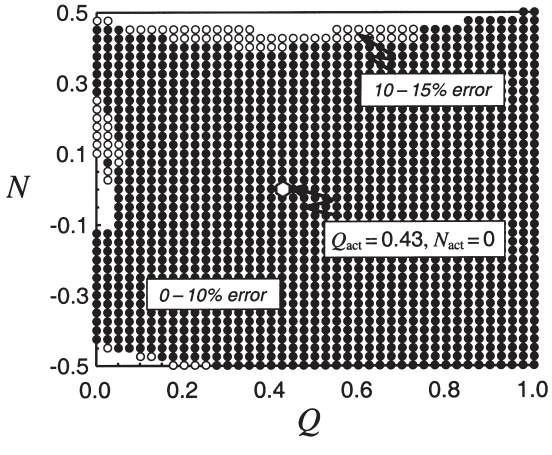

Fig. 15. Domain of convergence for the combined small and large indenter case. The size is significantly enlarged compared with the single indenter case (Fig. 13).

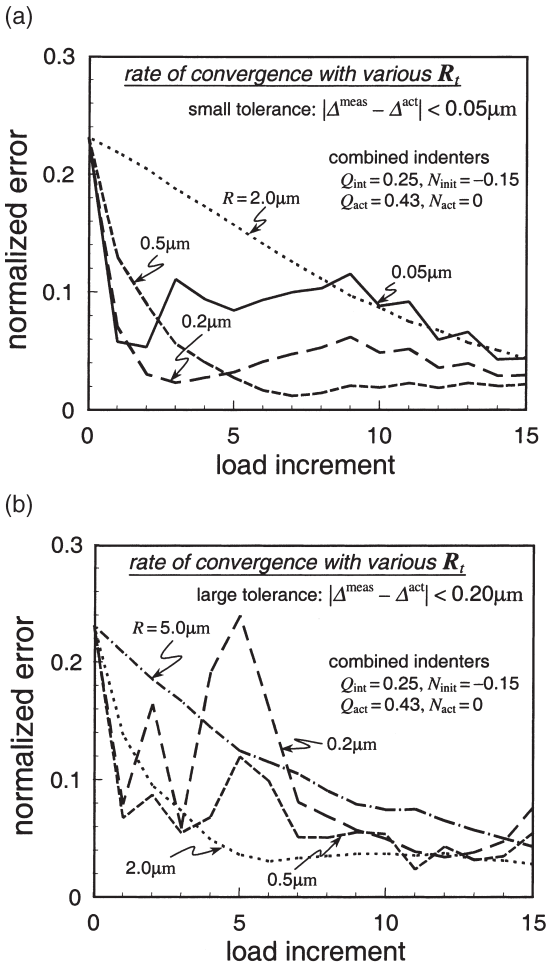

Fig. 17. Converging trends of the combined indenter case. Each curve is for different values in the error covariance matrix $\boldsymbol{R}_t$. The results are shown for the small and large measurement tolerance/error cases. (a) $|\Delta^{meas} - \Delta^{act}| < 0.05$ μm and (b) $|\Delta^{meas} - \Delta^{act}| < 0.20$ μm.

assigned, the convergence may be rapid but also unstable.

To investigate further the influence of R, we have carried out four additional calculations with larger measurement errors. The simulated P–Δ measurements with the tolerance $|\Delta_t^{err}|_{max} = 0.20$ μm, shown in Fig. 16(a), are used. The rate of convergence is shown in Fig. 17(b). With the larger measurement errors, the convergence of a given R is different from that shown in Fig. 17(a). However, in terms of relative magnitudes, the trends are very similar. A large R yields slow and steady convergence while a small R yields fast but unstable convergence. From inspection of both figures, the optimum value appears to be $R \sim 10|\Delta_t^{err}|_{max}$. This corresponds to $R = 0.5$ μm in Fig. 17(a) and $R = 2$ μm in Fig. 17(b). Each curve in the respective figure shows the optimal convergence trend.

6. SUMMARY

This paper introduces a new procedure based on inverse analysis and instrumented indentation. It has been known that more material information could be extracted from measured load–displacement curves. The present Kalman filter procedure is one of the means to maximize the usefulness of indentation data. For verification and optimization of the procedure, detailed finite element analyses are carried out to determine unknown parameters of elastic–plastic FGMs. Using the idealized model, the parameters that define the compositional variations and effective mechanical properties through the thickness are estimated by the inverse analysis. The former parameter is for the assumed power-law compositional distribution and the latter parameter sets the stress–strain transfer of modified rule-of-mixtures properties.

As in many inverse analyses, we found that the model is initially "ill-posed" or "ill-conditioned" (i.e., not able to achieve good convergence characteristics) with single indenter measurements. This problem is overcome by use of an additional indenter with a larger radius. In addition, it is shown that the Kalman filter is well suited for the present non-linear or elastoplastic problem since it processes over *multiple* load increments to best estimate the solutions. Although similar displacements are possible in models with different properties at a given load, models with different q and n should not continue to yield similar displacements at *various* loads. Required steps in the proposed procedure are summarized below.

1. Determine the material constants of homogeneous material separately. The ceramic and metal properties can be obtained by indentation procedures described in [17, 20].
2. Perform preliminary finite element calculations to determine suitable ranges of load increments for two differently sized indenters. The FGM parameters can be tentatively set at $Q = 0.5$ and $N = 0$. Use the finite element solutions to monitor approximate sizes of plastic zones.
3. Establish reference data from numerically generated P–Δ records with 16 different Q and N. Use cubic Lagrangian functions to interpolate the displacements and their gradients for each indenter.
4. Carry out instrumented indentation on the FGM layer using two indenters with different spherical radii.
5. Assign initial estimates of Q and N. Set values for $\boldsymbol{P}_0$ (with ΔQ, ΔN) and $\boldsymbol{R}_t$ (with $R = 10|\Delta^{err}|_{max}$ where $|\Delta^{err}|_{max}$ is the measurement error/noise bound).
6. Carry out the Kalman filter process for 15 increments to obtain the final estimates of Q and N.

One important question in the inverse analysis is how to identify the accuracy of the final estimates in

real tests where actual solutions are unknown. Although there is no direct method to judge the accuracy, we can propose the following procedure. First, carry out the Kalman filter with some initial estimates. Instead of terminating at this point, carry out another Kalman filter procedure. In the second attempt, the final estimates of the first attempt can be used as the initial estimates. This procedure can be repeated for a few times. If the final estimates are similar in all processes, then it is likely that they are close to the actual solutions. Alternatively, if the repeated procedures produce different final estimates, a different set of initial estimates must be used in the inverse analysis.

Implementation of the procedure for a real FGM specimen is being prepared currently. Although the proposed procedure is described for elastic–plastic FGMs, a similar procedure can be used to determine other parameters, including thickness, yield stress and anisotropic moduli, of any layers and coatings. Furthermore, the number of unknown parameters in the inverse analysis can be also increased. This aspect is currently being investigated.

Acknowledgements—The authors acknowledge the National Science Foundation for support of this work under award CMS-9800301. T. N. was also supported by the Army Research Office under grant DAAD19-99-1-0318. The helpful discussions with Professor Alan Kushner are also appreciated. The computations were carried out on HP7000/C180 and C360 workstations using the finite element code ABAQUS, which was made available under academic license from Hibbitt, Karlsson and Sorensen, Inc.

REFERENCES

1. Sampath, S., Herman, H., Shimoda, N. and Saito, T. *MRS Bull.*, 1995, **20**(1), 27.
2. Suresh, S. and Mortensen, A. *Fundamentals of Functionally Graded Materials*, IOC Communications Ltd, London, 1998.
3. Weissenbek, E., Pettermann, H. E. and Suresh, S. *Acta mater.*, 1997, **45**, 3401.
4. Suresh, S., Giannakopoulos, A. E. and Alcala, J. *Acta mater.*, 1997, **45**, 1307.
5. Giannakopoulos, A. E. and Suresh, S. *Int. J. Solids Struct.*, 1997, **34**, 2357.
6. Giannakopoulos, A. E. and Suresh, S. *Int. J. Solids Struct.*, 1997, **34**, 2393.
7. Williamson, R. L., Rabin, B. H. and Drake, J. T. *J. Appl. Phys.*, 1993, **74**, 1310.
8. Kesler, O., Finot, M., Suresh, S. and Sampath, S. *Acta Mater.*, 1997, **45**, 3123.
9. Jitcharoen, J., Padture, N. P., Giannakopoulos, A. E. and Suresh, S. *J. Am. Ceram. Soc.*, 1998, **81**, 2301.
10. Delale, F. and Erdogan, F. *J. Appl. Mech.*, 1988, **55**, 317.
11. Kalman, R. E. *ASME J. Basic Eng.*, 1960, **82D**, 35.
12. Grewal, M. S. and Andrews, A. P. *Kalman Filtering: Theory and Practice*, Prentice-Hall, Inc, New Jersey, 1993.
13. Hoshiya, M. and Saito, E. *J. Eng. Mech.*, 1984, **110**, 1757.
14. Ishida, R. *Trans. JSME, Part A*, 1994, **60**, 443.
15. Aoki, S., Amaya, K., Sahashi, M. and Nakamura, T. *Comp. Mech.*, 1997, **19**, 501.
16. Suresh, S. and Giannakopoulos, A. E. *Acta mater.*, 1998, **46**, 5755.
17. Giannakopoulos, A. E. and Suresh, S. *Scripta mater.*, 1999, **40**, 1191.
18. Jorgensen, O., Giannakopoulos, A. E. and Suresh, S. *Int. J. Solids Struct.*, 1998, **35**, 5097.
19. Alcala, J., Giannakopoulos, A. E. and Suresh, S. *J. Mater. Res.*, 1998, **13**, 1390.
20. Alcala, J., Gaudette, F., Suresh, S. and Sampath, S., *J. Mater. Res.*, submitted for publication.
21. Qian, G., Nakamura, T., Berndt, C. C. and Leigh, S. H. *Acta mater.*, 1997, **45**, 1767.
22. Sampath, S., Smith, W. C., Jewett, T. J. and Kim, H. *Mater. Sci. Forum*, 1999, **308**, 383.
23. Moretensen, A. and Suresh, S. *Int. Mater. Rev.*, 1995, **40**, 239.
24. Suresh, S. and Mortensen, A. *Int. Mater. Rev.*, 1997, **42**, 85.